Journal of Chromatography, 463 (1989) 51–71
Elsevier Science Publishers B.V., Amsterdam — Printed in The Netherlands

CHROM. 21 039

THE SEPARATION PROCESS IN ISOTACHOPHORESIS

II. BINARY MIXTURES AND TRANSIENT STATE MODELS

TAKESHI HIROKAWA*, KIYOSHI NAKAHARA and YOSHIYUKI KISO
Applied Physics and Chemistry, Faculty of Engineering, Hiroshima University, Shitami, Saijo, Higashi-hiroshima 724 (Japan)
(First received March 23rd, 1988; revised manuscript received September 12th, 1988)

SUMMARY

By the use of a multichannel ultraviolet-photometric zone detector, the separation processes in binary mixtures (monochloroacetic acid and picric acid, 4,5-dihydroxy-3-(*p*-sulphophenylazo)-2,7-naphthalenedisulphonic acid and monochloroacetic acid) were measured to obtain information about how the transient state is affected by the properties of the sample solution, such as the pH (pH_S), the concentration and the ratio of the constituent concentrations. It was found that the velocity of the mixed zone boundaries and the resolution time, t_{res}, of the binary systems were dependent on these properties to a considerable extent as previously reported for the chlorate–formate system by different authors. Some theoretical models are discussed to simulate the transient state. It is concluded by simulations that pH_S varies considerably at the initial stage of migration due to the influence of the buffer ion from the leading zone, namely the pH of the actually solution interfacing with the mixed zone formed is different from pH_S. The properties of the mixed zone are dependent not only on those of the sample but also on those of the leading zone. A good agreement was obtained between the observed and simulated t_{res} by considering this pH change.

INTRODUCTION

In order to study the dynamics of isotachophoretic separation, we constructed a 32-channel UV-photometric detection system and the design and the performance were reported in the preceeding paper[1]. The time to scan the 32 detectors per 16.5 cm was *ca.* 0.25 s and the high resolution allowed the accurate determination of the boundary velocities and the resolution time in the transient state.

Several studies have been reported concerning the analysis of the transient state. Brouwer and Postema[2] proposed a separation diagram and showed that the sample introduces a transient system of homogeneous zones which are finally reduced to the zones containing only one component of the sample. Vacik and Fidler[3] treated the transient state of a binary mixture theoretically by solving the differential equations of the separation. The transient state was also studied by Mikkers *et al.*[4,5] and the

0021-9673/89/$03.50

criterion of the separation was discussed in detail. Using the equations derived, they compared the simulated resolution time with the observed values. The most important conclusion of these studies was that for an isotachophoretic separation the ratio of the effective mobilities of the samples must be different from unity in the transient mixed zone, not at the steady state. Therefore the pH of the leading electrolyte is decisive for separation.

According to the theoretical approach of Mikkers *et al.*[4] in which the moving boundary equation was applied to the initial interface between the sample injected and the mixed zone formed, the separability was affected also by the properties of the sample solution such as the pH (pH_S), the concentrations and the effective mobilities of the constituents. We call the model proposed in the simulation by Mikkers *et al.*[4,5] the SPR (sample property reflecting) model hereafter. As discussed in ref. 5, the agreement between the simulated and the observed resolution time was very good when the samples were weak acids. However, for a mixture of weak and strong acids, the simulated pH_S dependence of the resolution time was overestimated. The SPR model was not present on the separation diagram proposed by Brouwer and Postema[2]. However the formulation of the SPR model is very persuasive and the discrepancy of 50% found for formic and chloric acids ($pH_S = 2.4$) may not be a problem from the practical viewpoint[5]; it probably suggests that a fundamentally important problem still remains in the SPR model.

As described in a later section, the theoretical estimates of the boundary velocities and the resolution time depend considerably on whether the velocity of the initial boundary between the solution injected and the mixed zone formed in the separation process is zero or not, in other words, whether the initial boundary can be treated as an ideal concentration boundary.

In this study, first the validity of the separation diagram proposed by Brouwer and Postema[2] was examined using a zone scanning analyzer. Next the resolution time and the boundary velocities of binary mixtures were measured accurately and compared with the theoretical estimates on the basis of some different physical models concerning the initial boundary in the separation process.

THEORETICAL

Assuming a binary mixture of constituents A and B, the stack configuration supposed at the transient state is the leading zone (L), A, the mixed zone AB, B and the terminating zone (T).

Brouwer and Postema[2] discussed the separation process in isotachophoresis and suggested a separation diagram of a binary mixture in a separation tube as illustrated in Fig. 1. On the basis of this simple model, an important relationship between the sample concentration in the steady state zones and that of the mixed zone can be derived, which is closely related with the resolution time, t_{res}.

The distance, D, of the boundaries from the sample-injected position (the initial interface between the sample solution injected and the leading zone) was expressed as a linear function of time, t,

$$D_{L/A} = V_{IP}t \tag{1}$$

$$D_{A/AB} = V_{A/AB}t \qquad t \leqslant t_{res} \tag{2}$$

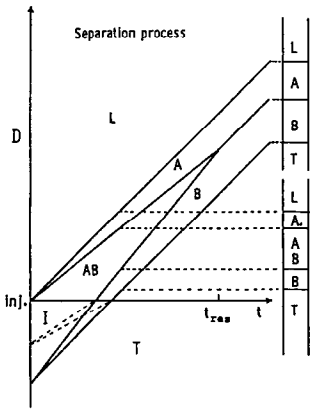

Fig. 1. Separation diagram for a binary mixture in a separation tube. D = Distance from injection port (inj); t = time; t_{res} = resolution time; I = zone of sample solution injected; L = leading zone; A, B = steady state zones; AB = mixed zone; T = terminating zone.

$$D_{A/B} = V_{IP}t - l_A \qquad t \geqslant t_{res} \tag{3}$$

$$D_{AB/B} = V_{AB/B}t - (l_A + l_B) \qquad t \leqslant t_{res} \tag{4}$$

$$D_{B/T} = V_{IP}t - (l_A + l_B) \tag{5}$$

where V_{IP} denotes the isotachophoretic velocity, $V_{A/AB}$ and $V_{AB/B}$ the velocity of the boundaries A/AB and AB/B and l_A and l_B are the zone lengths of components A and B at the steady state, which vary in proportion to the sample amount. We will call eqns. 1–5 the boundary functions hereafter. They express the solid lines in Fig. 1, where the zone length of the sample solution injected is equal to $l_A + l_B$. When the concentration is high keeping the sample amount constant, the separation process may follow the broken lines. The gradients of the broken lines depend on the sample concentration, however the separation diagram suggests that $V_{AB/B}$ and $V_{A/AB}$ are independent of the concentration of the sample solution. Therefore the behaviour of the zone boundaries in the transient state may be treated as illustrated by the solid lines in Fig. 1.

From the separation diagram, t_{res} can be expressed by the following equations:

$$t_{res} = l_A/(V_{IP} - V_{A/AB}) \tag{6}$$

or

$$t_{res} = l_B/(V_{AB/B} - V_{IP}) \tag{7}$$

As far as the separation diagram is valid, the values of t_{res} from eqns. 6 and 7 must coincide. A different expression of t_{res} can be obtained by eliminating V_{IP} from eqns. 6 and 7:

$$t_{res} = (l_A + l_B)/(V_{AB/B} - V_{A/AB}) \tag{8}$$

This equation can be derived also from the relationship $D_{A/AB} = D_{AB/B}$ at t_{res}. The velocity of the mixed zone boundaries can be derived from the moving boundary equation[6] as

$$V_{A/AB} = E_{AB}\bar{m}_{B,AB} \tag{9}$$

$$V_{AB/B} = E_{AB}\bar{m}_{A,AB} \tag{10}$$

where E_{AB} denotes the potential gradient of the mixed zone, $\bar{m}_{B,AB}$ and $\bar{m}_{A,AB}$ the effective mobilities of the constituents in the mixed zone.

The total amount of samples in the zone interposed by the L/A and B/T boundaries equals the amount injected, and is constant regardless of the separation process being at the transient state or at the steady state. Therefore the concentration of sample A in the mixed zone AB, $C^t_{A,AB}$, and that in the steady zone, $C^t_{A,S}$, can be correlated as:

$$(V_{IP} - V_{A/AB})tC^t_{A,S} + [V_{A/AB}t - V_{AB/B}t + (l_A + l_B)]C^t_{A,AB} = l_A C^t_{A,S} \tag{11}$$

The separation diagram suggested that eqn. 11 may be valid from $t = 0$ to $t = t_{res}$ irrespective of whether the zone length of the sample solution injected is equal to the sum $l_A + l_B$ or not. Then eqn. 11 can be reduced by inserting $t = 0$:

$$C^t_{A,AB} = l_A/(l_A + l_B)C^t_{A,S} \tag{12}$$

For component B, similarly:

$$C^t_{B,AB} = l_B/(l_A + l_B)C^t_{B,S} \tag{13}$$

Then the ratio of the concentrations is expressed as:

$$\frac{C^t_{B,AB}}{C^t_{A,AB}} = \frac{l_B C^t_{B,S}}{l_A C^t_{A,S}} \tag{14}$$

Eqn. 14 suggests that the ratio of the total concentrations of the sample constituents in the mixed zone is correlated with that of the sample amounts, and is completely independent of the properties of the initial sample solution. Hereafter we will refer to this transient model as the non-SPR model. As discussed in refs. 4 and 5, t_{res} depends strongly on the ratio $C^t_{B,AB}/C^t_{A,AB}$.

In the SPR model[4], on the other hand, the ratio was derived by applying the moving boundary equation[6] to the initial interface, namely, the boundary between the sample solution injected and the transient mixed zone. The moving boundary equation for component A can be written as

$$\frac{\bar{m}_{A,I}C^t_{A,I}E_I - \bar{m}_{A,AB}C^t_{A,AB}E_{AB}}{C^t_{A,I} - C^t_{A,AB}} = V_{I/AB} \tag{15}$$

where $\bar{m}_A$ denotes the effective mobility (the product of the mobility and the degree of

dissociation) of ion A, E the potential gradient, and the subscript I the zone of the sample solution injected. A similar equation can be written for component B:

$$\frac{\bar{m}_{B,I}C^t_{B,I}E_I - \bar{m}_{B,AB}C^t_{B,AB}E_{AB}}{C^t_{B,I} - C^t_{B,AB}} = V_{I/AB} \tag{16}$$

An assumption was made that the boundary is an ideal concentration boundary, namely the boundary velocity, $V_{I/AB}$, is null. Consequently, from eqns. 15 and 16, the following relationship was obtained:

$$\frac{C^t_{B,AB}}{C^t_{A,AB}} = \frac{\bar{m}_{A,AB}\bar{m}_{B,I}C^t_{B,I}}{\bar{m}_{B,AB}\bar{m}_{A,I}C^t_{A,I}} \tag{17}$$

The effective mobilities $\bar{m}_{A,I}$ and $\bar{m}_{B,I}$ in eqn. 17, hence $\bar{m}_{B,AB}$ and $\bar{m}_{A,AB}$ in eqns. 6–10, will depend on the pH of the sample solution, pH_S. Besides the concentration ratio, t_{res} depends on the relative mobility of the samples and buffer ions, the mobility of the leading ion, the dissociation constants, the degree of dissociation of samples in the mixed zone and those of the samples in the solution injected[4]. Therefore, even if the sample amount is constant, the SPR model demands that the resolution time depends on pH_S especially for the separation of a pair of weak and strong electrolytes.

The SPR formulation reported is applicable to a binary system, where the component ions are monovalent and the ionic strength of all zones is zero[4]. We extended the previous SPR model to treat multivalent ions by considering ionic strength as follows.

(1) The mobilities of the sample components A, B and the buffer ion Q were calculated on the basis of the dissociation constants and the pH of the mixed zone. For simplicity a monovalent buffer ion was assumed. At the first stage of iteration the pH of the mixed zone was assumed equal to the average of the pH values of the zones at the steady state.

(2) The potential gradient of the mixed zone, E_{AB}, was calculated from the following equation derived from the moving boundary equation for the boundary A/AB:

$$E_{AB} = \frac{\bar{m}_A E_A C^t_A}{\bar{m}_{A,AB}C^t_{A,AB} + \bar{m}_{B,AB}(C^t_A - C^t_{A,AB})} \tag{18}$$

(3) The total concentration of the buffer ion in the mixed zone, $C^t_{Q,AB}$, was calculated from the following equation derived from the moving boundary equation for the boundary A/AB:

$$C^t_{Q,AB} = \frac{\bar{m}_{Q,A}E_A + \bar{m}_{B,AB}E_{AB}}{(\bar{m}_{Q,AB} + \bar{m}_{B,AB})E_{AB}} \cdot C^t_{Q,A} \tag{19}$$

The partial concentration of the buffer ion at the pH was also calculated.

(4) From the electroneutrality relationship in the mixed zone, the concentrations of components A and B can be calculated as

$$C^{t}_{A,AB} = F_1/(F_2 + F_3F_4) \tag{20}$$

$$C^{t}_{B,AB} = C^{t}_{A,AB}F_4 \tag{21}$$

$$F_1 = -[C_H - C_{OH} + C^{t}_{Q,ABC}/(1 + k_Q/c_H)] \tag{22}$$

$$F_2 = \frac{\sum_{i=1}^{n_A} [z_{A,i}(\Pi k_{A,i})/C_H^i]}{1 + \sum_{i=1}^{n_A} (\Pi k_{A,i})/C_H^i} \tag{23}$$

$$F_3 = \frac{\sum_{i=1}^{n_B} [z_{B,i}(\Pi k_{B,i})/C_H^i]}{1 + \sum_{i=1}^{n_B} (\Pi k_{B,i})/C_H^i} \tag{24}$$

$$F_4 = \frac{\bar{m}_{B,I}C^{t}_{B,I}\bar{m}_{A,AB}}{\bar{m}_{A,I}C^{t}_{A,I}\bar{m}_{B,AB}} \tag{25}$$

where C_H and C_{OH} denote the concentrations of H^+ and OH^-, $C^{t}_{Q,ABC}$ the total concentration of buffer in the zone ABC, k_Q, k_A and k_B the acid dissociation constants, $z_{A,i}$ and $z_{B,i}$ the ionic charge of the ith constituent ion of component A and B, and n_A and n_B the numbers of the constituent ions. A monovalent cationic buffer was assumed in eqn. 22. The partial concentrations of the component ions at the pH were also calculated.

(5) The specific conductivity of the mixed zone, κ_{AB}, was calculated considering all ionic constituents in the mixed zone.

(6) The consistency of the current density was checked by the following RFQ function:

$$RFQ = (E_A\kappa_A/E_{AB}\kappa_{AB}) - 1 \tag{26}$$

Until RFQ was considered as zero (actually we used a threshold value of 10^{-5}), steps (1)–(6) were repeated by varying the pH of the mixed zone.

A computer program SIPSR was written in order to simulate the transient state according to the above procedure by modification of a program SIPS for the steady state analysis[7,8]. The above procedure was essentially the same as the previously proposed SPR model in principle. Actually the result obtained by SIPSR (see below) was very similar to that reported by Mikkers *et al*[5], when the SPR model was used. In SIPSR, however, the effect of the ionic strength on the mobility and dissociation constants was taken into account together with the contributions of H^+ and OH^- to the zone conductivity, all of which were neglected in refs. 4 and 5. By introducing these corrections, the algebraic expression of t_{res} cannot be given in a simple form. The value of t_{res} was obtained as a result of an iterative calculation. The non-SPR model using eqn. 14 instead of eqn. 17 for the ratio of the concentrations of the components in the

mixed zone can also be tested by SIPSR. As shown in this section, the dependences of pH_S on t_{res} in the non-SPR model and the SPR model will be different. The difference between the theoretical estimates obtained by these models will be discussed in a later section in comparison with the experimental results.

EXPERIMENTAL

The samples were 4,5-dihydroxy-3-(*p*-sulphophenylazo)-2,7-naphthalenedisulphonic acid (SPADNS), picric acid (PIC) and monochloroacetic acid (MCA). Except for MCA, these samples absorb visible and ultraviolet light. The sodium salt of SPADNS was obtained from Dojin in the most pure form. The other compounds were obtained from Tokyo Kasei (extra pure grade). Stock sample solutions (*ca.* 10 m*M*) were prepared by dissolving them in distilled water without further purification. As discussed later, the resolution time of PIC and MCA was measured by varying the pH of the mixture solution. The pH was adjusted to 2.5–3.7 by adding β-alanine. The pH measurements were carried out using a Horiba expanded pH meter, Model F7ss.

The leading electrolyte (hydrochloric acid) used was 5 and 10 m*M*. The pH was adjusted to 3.6 by adding β-alanine. The terminator was 5 and 10 m*M* caproic acid. Hydroxypropylcellulose (HPC, 0.2%) was added to the leading and terminating electrolytes to suppress electroendosmosis. The sample solution was injected into the terminating electrolyte near the boundary between the leading and the terminating electrolytes. The pH of the terminating electrolyte was also adjusted by β-alanine to ensure the pH of the sample solution at the initial stage of migration was equal to the prepared value. The separating tubes used were 0.51 mm I.D. and 1 mm O.D., and 0.54 mm I.D. and 1 mm O.D. All experiments were carried out at 25°C.

The data processing and the simulation were carried out by the use of NEC PC9801E and PC9801VX microcomputers. The figures were plotted by a Roland DG Model DXY-980.

TABLE I

PHYSICO-CHEMICAL CONSTANTS USED IN SIMULATION (25°C)

m_0 = Absolute mobility ($cm^2\ V^{-1}\ s^{-1}$) · 10^5; pK_a = thermodynamic acid dissociation constants, assumed value being used for Cl^-.

Ion	m_0	pK_a
Cl^-	79.08	−2
β-Alanine$^+$	36.7*	3.552
GABA$^+$	30**	4.03
Histidine$^+$	29.7	6.04
Formate$^-$	56.6	3.752
Glycolate$^-$	42.4	3.886
ClO_3^-	67.0	−2.7
Monochloroacetate$^-$	41.1*	2.865
Picrate$^-$	31.5	0.708

* The mobilities were obtained by our isotachophoretic method or conductivity measurement. The other mobilities and pK_a values are taken from ref. 9.

** γ-Aminobutyric acid, ref. 5.

RESULTS AND DISCUSSION

Under the electrolyte condition used, the samples were detected in the order of SPADNS, MCA and PIC. The simulated effective mobilities, $\bar{m}$, at the steady state were $47.7 \cdot 10^{-5}$, $35.1 \cdot 10^{-5}$ and $29.3 \cdot 10^{-5}$ $cm^2\ V^{-1}\ s^{-1}$, and the R_E values ($R_E = \bar{m}_L/\bar{m}_S = E_S/E_L$, where E is the potential gradient, and L and S the leading and sample ions, respectively) were 1.59, 2.16 and 2.59 respectively. Table I shows the m_0 and pK_a values of the samples and electrolyte constituents used in the simulations.

Separation diagram

First the boundary functions (eqns. 1–5) were determined for a 1:1 mixture of SPADNS(S) and MCA(M) to compare with the separation diagram (Fig. 1). These functions can be determined accurately by the least-squares method using the exact positions of the photocells and the times when the boundaries passed each cell. The sample concentration was varied in the range of 1.25–10 m*M*. A small amount of PIC was added to the mixture to distinguish the UV-transparent terminating zone. When the sample concentration was 2.5 m*M* and the concentration of the leading electrolyte was 10 m*M*, the zone length of the solution injected was almost equal to the sum of the zone lengths of the separated samples at the steady state. In this case, the separation processes expected were those illustrated in Fig. 1 by the solid lines.

Fig. 2. shows the transient isotachopherograms obtained for the 1.25 (A) and 10 m*M* (B) mixtures respectively. The sample amount was 60 nmol and pH_S = *ca.* 2.5. The time-based zone lengths at the steady state were 377.9 and 380 s respectively. The boundaries between the leading and the SPADNS zones were rearranged at the same abscissa position. The mixed zone observed was that of SPADNS and MCA. The small peak adjacent to the terminating zone was due to the absorption of PIC. The zone

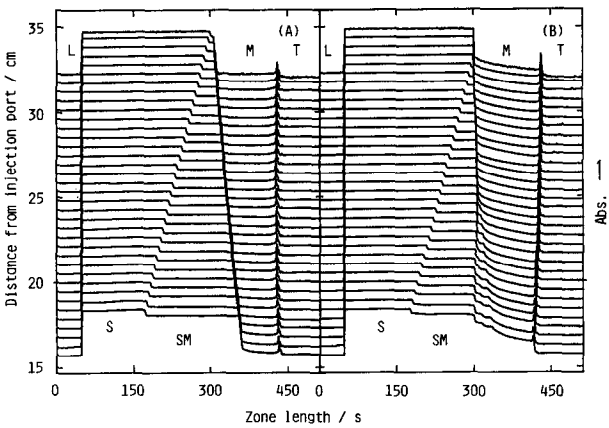

Fig. 2. Transient isotachopherogram of SPADNS and monochloroacetic acid observed by the use of the 32-channel UV-photometric detector. The sample concentration was 1.25 (A) and 10 m*M* (B). The sample amount was 60 nmol. The position of the baselines of the UV absorption shows the distance of the photocell from the sample injection port. The migration current was 98.4 μA. The leading electrolyte was 10 m*M* hydrochloric acid and the pH was adjusted to 3.6 (buffer β-alanine). The terminator was 10 m*M* caproic acid.

imposed by the peak and the mixed zone (SM) is that of MCA (M). The time-based zone lengths of the whole sample zones were almost constant during detection. In such cases, the correlation coefficients obtained in the linear least-squares fitting were better than 0.99999 for all boundary functions; the value 1 was obtained frequently. The observed pherograms for 2.5 and 5 m*M* samples were very similar to that for 1.25 m*M*.

When the 10 m*M* mixture was analyzed, as shown in Fig. 2B, loose boundaries were observed between the SM and M zones with high reproducibility. Such loose boundaries were never observed at the boundary S/SM. Besides the uniform mixed zone, it is apparent from the UV absorption that the MCA zone was contaminated with a considerable amount of SPADNS, although this amount decreased gradually with time. This phenomena was found also in the 5-m*M* case, but to a much smaller extent. In such cases the linearity of the boundaries L/S and S/SM was as good as that for the dilute samples, however that of the boundaries SM/M and M/T was slightly worse. From Fig. 2, the so-called mixed zone found in the 10-m*M* case diminished more rapidly than in that of the 1.25-m*M* case. However, a considerable amount of SPADNS still remained in the MCA zone after the mixed zone had diminished.

The cause of the loose boundaries in the 10 m*M* mixture (the different types of concentration boundaries which are not shown in Fig. 1) can be elucidated as follows: the sample solution injected mixed partially with the terminating electrolyte and the resulting solution was not homogeneous in concentration. The potential gradient in the initial solution decreases with increasing concentration, therefore a longer period will be necessary to reject, *e.g.*, terminating ions from the initial zone when the concentrated sample is analyzed. For the diluted mixtures, the inhomogeneities of the initial solution will diminish rapidly and the observed transient state can be regarded as an ideal pattern in the ideal binary system. Thus the transient state observed for the 10

TABLE II

DEPENDENCE OF SAMPLE CONCENTRATION ON THE OBSERVED RELATIVE BOUNDARY VELOCITY AND THE INTERCEPTS OF THE BOUNDARY FUNCTIONS FOR THE SPADNS–MONOCHLOROACETATE SYSTEM (1:1)

Time-based zone length is normalized to 300 s. Operational system: leading electrolyte 10 m*M* hydrochloric acid–*β*-alanine (pH 3.60); current = 98.4 *μ*A; diameter of the separation tube = 0.51 mm; sample amounts (S, M) each 20.0 nmol (S = SPADNS, M = monochloroacetic acid). V_R = relative velocity (boundary velocity/V_{IP}); D_0 = intercepts of the boundary function (mm).

	Concentration of samples (mM)			
	1.25	*2.5*	*5*	*10*
$V_{R,S/SM}$	0.798 ± 0.002	0.796 ± 0.003	0.798 ± 0.005	0.791 ± 0.004
$V_{R,SM/M}$	1.105 ± 0.003	1.088 ± 0.005	1.071 ± 0.007	1.046 ± 0.007
$V_{R,M/T}$	1.004 ± 0.003	1.006 ± 0.005	0.984 ± 0.005	0.977 ± 0.005
$D_{0,L/S}$*	0	0	0	0
$D_{0,S/SM}$	0.7 ± 0.3	1.1 ± 0.5	1.9 ± 0.9	− 0.3 ± 0.7
$D_{0,S/M}$	− 67.8 ± 1.5	−68.1 ± 2.4	−60.2 ± 2.2	−58.0 ± 2.3
$D_{0,SM/M}$	−101.3 ± 1.2	−96.5 ± 2.0	−86.4 ± 2.4	−76.4 ± 3.2
$D_{0,M/T}$	− 98.6 ± 1.2	−97.4 ± 1.5	−90.4 ± 1.9	−90.7 ± 1.9

* The position of injection port is the frame of reference.

mM solution in the present experiments cannot simply be compared with those for the 1.25, 2.5 and 5 mM solutions.

Table II summarizes the dependences of the sample concentration on the relative boundary velocity, V_R, and the intercepts of the boundary functions, D_0. The intercepts were normalized to the time-based zone length of 300 s, which corresponded to the absolute zone length of 97 mm in the separating tube (I.D. = 0.51 mm). $V_{R,SM/M}$ decreased with increasing sample concentration, while that of S/SM was kept almost constant. If the migration model in Fig. 1 is valid, the intercepts of the boundary functions of L/S and S/SM should be zero (eqns. 1 and 2). In the present work this was valid considering the probable error. The intercepts of the boundary functions of SM/M and M/T (eqns. 4 and 5) also must coincide with each other and in this case the value should be −97 mm. When the sample concentration was 1.25 and 2.5 mM, these conditions were satisfied approximately. At higher concentrations, however, the conditions were not satisfied.

The conclusion is that the migration model in Fig. 1 is valid to a first approximation. Although the observed discrepancy between the intercepts of the SM/M and M/T boundary functions suggested a limitation of the model, so far we cannot deny the non-SPR model absolutely because the discrepancy was small. Another important conclusion was that the use of eqn. 6 is adequate for the evaluation of t_{res}. However the use of eqns. 7 and 8 is not always adequate for practical samples, since the boundary functions of the AB/B and B/T zones are easily perturbed by the mixing with the terminator.

It may be interesting to compare how different are the estimations of the separation process obtained by the non-SPR and the SPR models. Therefore we simulated the boundary velocities and resolution times of some binary systems by use of the models and compared them with the observed values.

Dependence of sample properties on the separation process

As already mentioned, the only difference between the SPR model and the non-SPR model is the expression for the ratio of the constituent concentrations, $C^{\downarrow}_{B,AB}/C^{\downarrow}_{A,AB}$, which are given by eqns. 14 and 17. Eqn. 14 of the non-SPR model contains only the zone length and the sample concentration at the steady state. On the other hand, eqn. 17 contains the effective mobility and the concentrations of the constituents both in the initial solution and in the mixed zone AB.

When the pK_a values of the samples are equal, in the SPR model, $\bar{m}_{A,I}$ and $\bar{m}_{B,I}$ in eqn. 17 vary in a similar manner corresponding to the pH of the sample solution, pH$_S$. Therefore t_{res} will be hardly affected by the variation of pH$_S$. This estimation by the SPR model has been verified by the observation of t_{res}[5] for glycolic acid (pK_a = 3.83) and formic acid (pK_a = 3.752)[9]. The agreement was very good and the deviations were 2–10% in the range pH 2.5–4.3. This system was studied first.

Mikkers *et al.* introduced the concept of the separation number, S, which enables the criterion of separation irrespective of the instrumental condition except for the migration current, i

$$S = \frac{F}{i} \cdot \frac{\partial n_A}{\partial t} = \frac{F}{i} \cdot \frac{n_A}{t_{res}} \tag{27}$$

where F is the Faraday constant and n_A the sample amount of constituent A. Table III summarizes t_{res} and S simulated by the Mikkers SPR model (SPR-I), the present SPR model (SPR-II), the non-SPR model and the observed values[5]. Apparently the agreement is good. The slight difference observed between SPR-II and SPR-I is due to whether the ionic strength correction was considered or not. For such a binary system, it is apparent that the SPR and the non-SPR are both useful for the transient state analysis. The simulated S value in ref. 5 for this system was 0.100 and which is 20% smaller than the present result. From the good agreement in the formate–chlorate system shown below, the discrepancy was attributed to the difference between the absolute mobility of glycolate used. This mobility was not cited in ref. 5. The estimated mobility to give $S = 0.1$ was $45 \cdot 10^{-5}$ cm^2 V^{-1} s^{-1}.

Then, the S and t_{res} observed[5] for a pair of strong acid and weak acid (chloric acid, $pK_a < 1$; and formic acid, $pK_a = 3.752$) were compared with the simulated values (Table III). The significant dependence of pH_S on S and t_{res} was simulated by the SPR model (<70%); on the other hand, no pH_S dependence was simulated by the non-SPR model. The observed pH_S dependence was less than 25% in the pH range. It is apparent that the non-SPR model is not suitable to simulate the observed pH_S dependence, however the S and t_{res} simulated by the non-SPR model agreed well with those by the SPR model at relatively high pH_S. Thus the transient state estimated by the non-SPR model is essentially the same as that estimated by the SPR models at high pH_S. In other words, the validity of eqn. 14 derived from the separation diagram in Fig. 1 depends on the pH_S.

TABLE III

SIMULATED AND OBSERVED SEPARATION NUMBER AND RESOLUTION TIME FOR FORMATE–GLYCOLATE AND CHLORATE–FORMATE SYSTEMS (1:1)

Operational system: leading electrolyte 10 mM hydrochloric acid–γ-aminobutyric acid (GABA, pH 4.03); current = 80 μA; diameter of the separation tube = 0.45 mm; sample amount = 100 nmol. S = separation number, see text; t_{res} = resolution time.

pH of sample	*Simulated*						*Observed*	
	*SPR-I**		*SPR-II***		*Non-SPR***		S	t_{res}***
	S	t_{res}	S	t_{res}	S	t_{res}		
Formate–glycolate system								
2.5	0.119	1014	0.124	972	0.113	1065	0.098	1230
3.0	0.118	1025	0.123	980	0.113	1065	0.098§	1230
3.5	0.115	1050	0.120	1003	0.113	1065	0.097§	1240
4.0	0.111	1088	0.116	1037	0.113	1065	0.095§	1270
Chlorate–formate system								
2.4	0.276	437	0.270	447	0.154	782	0.179	674
3.0	0.244	493	0.236	512	0.154	782	0.170§	709
3.5	0.202	597	0.193	624	0.154	782	0.155§	778
4.0	0.165	732	0.160	754	0.154	782	0.142§	849

* Mikkers formulation was used (ionic strength = 0).

** Present formulation, ionic strength was considered.

*** Estimated from S.

§ From Fig. 3 in ref. 5.

The cause of the overestimation of the pH_S dependence by the SPR model has been explained by the fact that the model made no allowance for the influence of a relatively high proton concentration at low pH_S and the functioning as a mobile counter constituents will decrease the efficiency of separation[5]. The elucidation may not be suitable in this case because the resolution times of the weak acid mixtures were observed under similar pH_S conditions. Moreover, in our SPR model (SPR-II), the influence of the proton was considered in the evaluation of the zone conductivity, however the simulated t_{res} values were essentially the same as those obtained with Mikkers SPR model (SPR-I) as shown in Table III.

Then the assumptions made in the SPR formulation were examined by simulation. The most important assumption was that the initial interface between the sample solution injected and the gradually formed mixed zone (I/AB) is treated as the ideal concentration boundary, namely the boundary is solvent-fixed. The other important assumption was that the pH of the sample solution injected was kept constant during analysis.

Mikkers *et al.*[4] suggested that it is not necessary to incorporate the hydrogen constituent into the moving boundary equation, quoting the literature[10–13]. When E_I in eqns. 15 and 16 is calculated from the zone conductivity of the injected solution for the evaluation of $V_{I/AB}$, therefore, two different ways were used. First the calculation was carried out as usual considering all ionic species in the injected solution: the partial contribution of H^+ to the conductivity was evaluated by $C_H\bar{m}_H F$ (C_H = concentration of H^+, $\bar{m}_H$ = mobility of H^+, F = Faraday constant). Next, the contribution of H^+ was evaluated by $C_H\bar{m}_Q F$ ($\bar{m}_Q$ = mobility of buffer). Table IV summarizes the

TABLE IV

SIMULATED VELOCITY OF THE BOUNDARY BETWEEN THE INJECTED SAMPLE ZONE AND THE MIXED ZONE FORMED FOR CHLORATE–FORMATE SYSTEM (1:1)

For the operational system see Table III. Simulated isotachophoretic velocity = 0.3732 mm/s. Cond. = simulated conductivity of the sample solution injected. E_I = Potential gradient of the sample solution injected.

	Contribution of H^+ to zone conductivity							
	*Strictly evaluated**				*Approximated**			
pH of sample	*Cond. ($mS\,cm^{-1}$)*	*E_I ($V\,cm^{-1}$)*	*Velocity ($mm\,s^{-1}$)*		*Cond. ($mS\,cm^{-1}$)*	*E_I ($V\,cm^{-1}$)*	*Velocity ($mm\,s^{-1}$)*	
			Chlorate	*Formate*			*Chlorate*	*Formate*
Sample concentration = 50 mM								
2.5	5.33	9.44	−0.0113	−0.0005	4.36	11.5	0.0042	0.0002
3.0	5.06	9.95	−0.0008	−0.0001	4.75	10.6	0.0038	0.0005
3.5	5.63	8.94	0.0022	0.0007	5.53	9.10	0.0033	0.0011
4.0	6.48	7.76	0.0026	0.0015	6.45	7.80	0.0028	0.0016
Sample concentration = 10 mM								
2.5	1.92	26.3	−1.3210	−0.0089	0.92	54.4	0.0879	0.0006
3.0	1.32	38.2	−0.2763	−0.0110	1.00	50.1	0.0442	0.0018
3.5	1.27	39.6	−0.0308	−0.0576	1.17	43.0	0.0236	0.0044
4.0	1.41	35.7	0.0058	0.0294	1.38	36.5	0.0157	0.0080

* For explanation, see text.

velocities of the boundary I/AB for the chlorate–formate system (50 and 10 mM) evaluated by eqns. 15 and 16, when the pH_S was varied in the range of 2.5–4. Apparently the volocities of the boundary I/AB were small enough when the sample concentration was 50 mM and E_I was evaluated by use of $C_H\bar{m}_QF$. However, unacceptably large values were simulated at low pH_S, when the exact E_I was used and the concentration of the mixture was 10 mM. Although the boundary velocities of the mixed zones and t_{res} are not affected by the concentration of the samples injected according to the present transient state models, the validity of the assumption used was lost for the dilute samples. Even if E_I was evaluated by use of $C_H\bar{m}_QF$, the simulated $V_{I/AB}$ from the concentration of chloric acid became so large that it could no longer be disregarded compared to $V_{I/AB}$ from that of formic acid. A similar situation was simulated when the non-SPR model was used.

The above simulation may suggest that $V_{I/AB}$ was not strictly zero when the concentration of H^+ was considered. Far from $V_{I/AB} = 0$, a rapidly moving pH boundary may exist in the initial sample zone. Namely, the pH of the solution actually interfacing with the mixed zone formed may vary significantly from the pH_S at the initial stage of migration. If this estimation is valid, the overestimation of the increasing separability at low pH_S by the SPR model can be elucidated properly. Although we did not observe the initial stage of migration by the present apparatus, this phenomenon is very plausible.

On the basis of these simulations, we incorporated the initial pH change in the SPR model. The velocity of the buffer ions (Q) toward the terminating side in the initial solution can be written as

$$V_{Q,I} = E_I\bar{m}_{Q,I} \tag{28}$$

where E_I denotes the potential gradient of the solution injected and $\bar{m}_{Q,I}$ the effective mobility of the buffer ion. A zone (I*) of which the pH is different from pH_S is considered between the injected position and the boundary moving with velocity $V_{Q,I}$. The counter ion from the leading electrolyte migrates into this zone immediately after starting migration. Then, on the assumption that the velocity of the boundary between the zone I* and the mixed zone is zero and the same kind of buffer ions are contained in the sample and the leading electrolyte, the following equation for the concentration of the counter ions in the sample zone, $C^t_{Q,I}$*, may be valid from the continuity principle

$$C^t_{Q,I}{}^* = E_L\bar{m}_{Q,L}C^t_{Q,L}/E_I\bar{m}_{Q,I} + C^t_{Q,I} \tag{29}$$

where E_L denotes the potential gradient of the leading zone, $\bar{m}_{Q,L}$ the effective mobility of the buffer ions in the leading zone, $C^t_{Q,L}$ the total concentration and $C^t_{Q,I}$ the concentration of the buffer ion in the injected samples. Apparently, eqn. 29 suggests that the pH of the solution actually interfacing with the mixed zone will be higher in an anionic separation. Therefore the concentration ratio (eqn. 17) estimated from the formed zone I* will be different from that obtained by the use of pH_S. We call this model SPR-III hereafter.

Table V shows the pH_S dependence of the simulated t_{res} and S for chlorate–formate system. Fig. 3 also shows the pH_S dependence of the observed[5] and simulated S. Apparently the agreement is quite good, confirming the validity of the model

TABLE V

OBSERVED AND SIMULATED SEPARATION NUMBER AND RESOLUTION TIME FOR THE CHLORATE–FORMATE SYSTEM (1:1) BY CONSIDERING THE INITIAL pH CHANGE (SPR-III)

OS = Operational systems: for I, see Table III. II = buffer β-alanine, pH_L = 3.60; III = buffer histidine, pH_L = 6.02. Sample amount = 100 nmol. pH_S = pH of the sample solution injected. pH_S* = Simulated pH of the solution actually interfacing with the mixed zone. Sim. = Value simulated by SPR-III model. Dev. (%) = Percent deviation.

OS	pH_S	pH_S*	*S*			t_{res}		
			*Obs.**	*Sim.*	*Dev. (%)*	*Obs.**	*Sim.*	*Dev. (%)*
I	2.4	3.75	0.179	0.174	−2.8	674	692	2.7
I	3.0	3.84	0.170	0.169	−0.6	709	716	1.0
I	3.5	4.09	0.155	0.156	0.6	778	773	−0.6
I	4.0	4.43	0.142	0.145	2.1	849	830	−2.2
II	2.4	3.43	0.259	0.250	−3.5	466	482	3.4
III	2.4	4.14	0.075	0.070	−6.7	1608	1717	6.8

* Observed values from ref. 5.

SPR-III. The simulated values of $E_l\bar{m}_{Q,l}$ were $2.18 \cdot 10^{-2}$ and $1.05 \cdot 10^{-2}$ mm/s in the case of pH_S = 2.4 and 4.0 respectively (migration current = 80 μA, I.D. of the separation tube = 0.45 mm). The simulated isotachophoretic velocity was 0.373 mm/s. As shown, the simulated pH shift was large (1.7–0.4). The shift reduced considerably the pH_S effect estimated by SPR-II, where the sample pH was kept constant during the separation.

Table VI shows the simulated R_E values, effective mobilities and concentrations of the zone constituents of the chlorate–formate system at both the steady state and the transient state. A significant difference between the models used was found only for the estimates of the sample concentrations in the mixed zone.

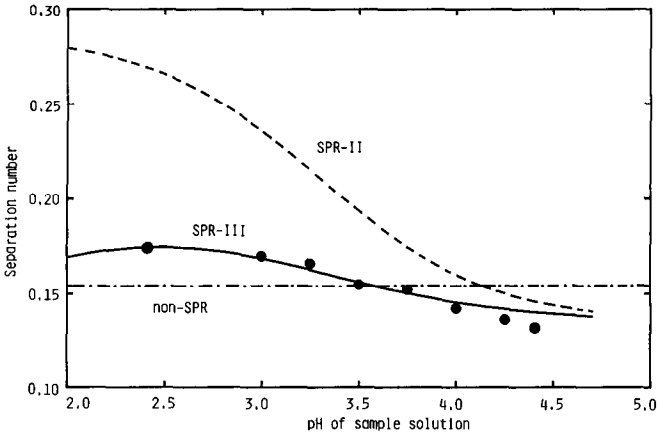

Fig. 3. The observed (●) and simulated separation number for the chlorate–formate system. The observed values were taken from ref. 5. For the operational system, see Table III. For the definitions of the transient state models, see text.

TABLE VI

SIMULATED R_E VALUES, EFFECTIVE MOBILITIES AND CONCENTRATIONS IN THE SEPARATION OF THE CHLORATE–FORMATE SYSTEM AT pH_L = 4.03 (25°C)

pH_S = pH of sample solution injected. R_E = Ratio of potential gradients, $E_{Sample}/E_{Leading}$. $\bar{m}_{CHL}$, $\bar{m}_{FOR}$ = Effective mobilities of chlorate (CHL) and formate (FOR) ions ($cm^2\ V^{-1}\ s^{-1}$) · 10^5. pH = pH of zones at the steady and transient states. C^t_{CHL}, C^t_{FOR} = Total concentrations (mM) of chlorate and formate. C^t_Q = Total concentration (mM) of buffer (β-Ala). $\bar{m}_Q$ = Effective mobility of buffer ($cm^2\ V^{-1}\ s^{-1}$) · 10^5. I = ionic strength · 10^3.

	pH_S	R_E	pH	$\bar{m}_{CHL}$	$\bar{m}_{FOR}$	C^t_{CHL}	C^t_{FOR}	$\bar{m}_Q$	C^t_Q	I
Steady state zone										
Chlorate		1.19	4.054	63.0	–	9.49	–	13.7	18.4	9.49
Formate		1.80	4.264	–	41.5	–	8.97	10.6	17.8	7.00
Transient mixed zone										
Non-SPR*	–	1.46	4.173	63.2	39.4	4.62	4.62	11.9	18.1	8.05
SPR-II	2.4	1.22	4.073	63.0	36.9	8.81	0.65	13.4	18.3	9.26
SPR-II	4.0	1.45	4.169	63.2	39.3	4.81	4.44	11.9	18.1	8.10
SPR-III	2.4	1.42	4.158	63.2	39.1	5.30	3.97	12.1	18.1	8.23
SPR-III	4.0	1.48	4.180	63.3	39.6	4.32	4.90	11.8	18.1	7.97

* For definitions of the transient state models, see text.

The applicability of the SPR models and the non-SPR model was examined for the different pair of a weak and a strong electrolyte, monochloroacetic acid (MCA: pK_a = 2.865, m_0 = 41.1 · 10^{-5} $cm^2\ V^{-1}\ s^{-1}$) and picric acid (PIC: 0.708, 31.5 · 10^{-5}). The pH_S dependence of both the velocity of the mixed zone boundaries and t_{res} was observed by the use of the multichannel UV detection system. Plots of the effective mobility *vs.* pH_S for these samples cross at pH *ca.* 3.4 and such a pair was called the reversed pair[4]. The pH_S was varied in the range of 2.5–3.7. The pH range is

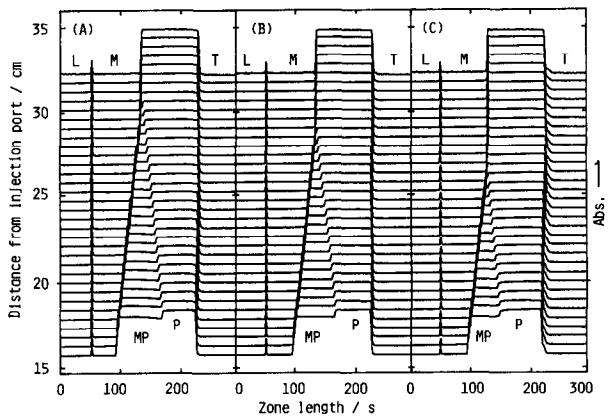

Fig. 4. Transient isotachopherogram of monochloroacetic acid (MCA) and picric acid (PIC) obtained by the use of the 32-channel UV-photometric detector. The pH of the sample solution was 2.5 (A), 3.0 (B) and 3.6 (C). The sample amount was 17.5 nmol (MCA) and 16.3 nmol (PIC). The migration current was 49.2 μA. The leading electrolyte was 5 mM hydrochloric acid and the pH was adjusted to 3.6 (buffer β-alanine). The terminator was 10 mM caproic acid. For pherograms, see Fig. 2.

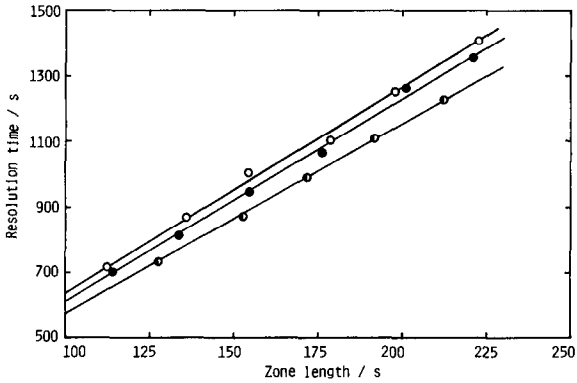

Fig. 5. The pH_S dependence of the resolution time *vs.* the whole time-based zone length in the monochloroacetic acid–picric acid system. For the operational system, see Fig. 4. pH_S = 2.5 (○), 3.0 (●) and 3.6 (◐).

sufficiently wide to study the present problem, since the degree of dissociation of MCA varies from 0.32 to 0.86 and $\bar{m}_{MCA,I}$ ($\bar{m}_{A,I}$ in eqn. 17) varies from $12 \cdot 10^{-5}$ to $33 \cdot 10^{-5}$ $cm^2\ V^{-1}\ s^{-1}$. The degree of dissociation of PIC and $\bar{m}_{PIC,I}$ ($\bar{m}_{B,I}$ in eqn. 17) is almost constant in this pH range and the values are *ca.* 1 and $29 \cdot 10^{-5}$ $cm^2\ V^{-1}\ s^{-1}$.

Fig. 4 shows the observed transient isotachopherogram of MCA (16 nmol) and PIC (16 nmol) at pH_S = 2.5, 3.0 and 3.6. A small amount of SPADNS was added to the mixture. The boundaries between the leading and SPADNS (small peaks in Fig. 4) zones were rearranged at the same abscissa position to demonstrate clearly the change in the individual zone length at the transient state. The observed overall time-based zone lengths were 154.4, 154.7 and 152.6 s respectively. These were the averaged values after the mixed zone had diminished. The t_{res} was given by eqn. 6. It may be evaluated by the following equation obtained by replacing the absolute zone length by the time-based zone length and the absolute velocity by the relative velocity ($V_R = V_{boundary}/V_{IP}$)

$$t_{res} = t_M/(1 - V_{R,M/MP}) \tag{6'}$$

where t_M is the time-based zone length of MCA. Eqns. 6 and 6′ are valid providing the intercepts of eqns. 1 and 2 are equal (zero). However, as already shown in Table II for the SPADNS–MCA system, a slight difference between the intercepts was observed in the MCA–PIC system, and this difference considerably affects the resolution time. Therefore we solved the following simultaneous boundary functions of M/MP and M/P:

$$D_{M/MP} = V_{M/MP}t + D_{0,M/MP} \tag{2'}$$

$$D_{M/P} = V_{IP}t + D_{0,M/P} \tag{3'}$$

When eqn. 3′ was not available because of a relatively large sample amount, the following equation for the boundary MP/P was used instead:

$$D_{MP/P} = V_{MP/P}t + D_{0,MP/P} \quad (4')$$

The boundary velocities and the intercepts in these equations were determined by the least-squares method. The resolution times in Fig. 4 were 1004, 946 and 871 s respectively and the experimental error was less than *ca.* ±20 s.

Fig. 5 shows t_{res} *vs.* the whole zone length at pH_S = 2.5, 3 and 3.6. The best-fitted linear functions were

$$\begin{aligned} t_{res} &= 6.33\ t_{zone} + 5.1 \quad pH_S = 2.5 \\ t_{res} &= 6.18\ t_{zone} - 4.7 \quad pH_S = 3.0 \\ t_{res} &= 5.81\ t_{zone} - 5.3 \quad pH_S = 3.6 \end{aligned} \quad (30)$$

where t_{zone} is the time-based zone length of the whole sample. Apparently t_{res} depends on pH_S, however the change was within *ca.* 10% in the pH range.

Table VII shows the simulated and the observed velocity of the mixed zone boundaries relative to the isotachophoretic velocity together with t_{res}. Apparently the values simulated by SPR-III agreed well with those observed. The discrepancy between the observed and the t_{res} simulated by the non-SPR model was always less than 20%. It should be noted that the non-SPR approach coincides with the SPR approach when pH_S is relatively high.

The relative velocity of the boundaries M/MP and MP/P may be expressed from eqns. 9 and 10 as:

$$V_{R,M/MP} = \bar{m}_{P,MP}E_{MP}/V_{IP} \quad (9')$$

$$V_{R,MP/P} = \bar{m}_{M,MP}E_{MP}/V_{IP} \quad (10')$$

TABLE VII

SIMULATED AND OBSERVED RELATIVE VELOCITY OF THE MIXED ZONE BOUNDARIES AND RESOLUTION TIME IN THE MONOCHLOROACETATE–PICRATE SYSTEM (1:1) AT pH_S = 2.5, 3.0 AND 3.6

Operational system: leading electrolyte 5 m*M* hydrochloric acid–β-alanine (pH 3.60); current = 49.2 μA; diameter of the separation tube = 0.51 mm; sample amounts, monochloroacetic acid (M) 20 nmol, picric acid (P) 19.87 nmol.

pH_S		*Simulated**			*Observed***
		Non-SPR	*SPR-II*	*SPR-III*	
2.5	$V_{R,M/MP}$	0.916	0.955	0.919	0.924 ± 0.003
	$V_{R,MP/P}$	1.099	1.148	1.104	1.087 ± 0.007
	t_{res}(s)	1054	1981	1102	1229 (1168)
3.0	$V_{R,M/MP}$	0.916	0.932	0.918	0.920 ± 0.002
	$V_{R,MP/P}$	1.099	1.120	1.103	1.083 ± 0.006
	t_{res}(s)	1054	1312	1089	1191 (1110)
3.6	$V_{R,M/MP}$	0.916	0.918	0.915	0.918 ± 0.001
	$V_{R,MP/P}$	1.099	1.102	1.098	1.067 ± 0.005
	t_{res}(s)	1054	1080	1041	1119 (1083)

* For definitions of the transient state models, see text.

** Probable error of velocity ratio was calculated from six experiments. The values in parentheses were calculated by eqn. 6'.

The effective mobility of picric acid, $\bar{m}_P$, is not affected by pH_S but that of monochloroacetic acid, $\bar{m}_M$, is affected. Therefore the observed decrease of $V_{R,M/MP}$ in Table VII suggested that E_{MP} decreased slightly with increasing pH_S.

Table VIII summarizes the simulated pH_S dependence on several parameters of the mixed zone, where E_{MP} was expressed as the ratio to the potential gradient of the leading zone ($R_{E,MP} = E_{MP}/E_L$). The slight decrease in $R_{E,MP}$ with increasing pH_S was simulated by the SPR models. According to this simulation, the pH of the mixed zone was almost independent of the change in pH_S. As mentioned before, therefore, the exact evaluation of the concentration ratio of the sample constituents, $C^t_{P,MP}/C^t_{M,MP}$, and E_{MP} are decisive for the simulation of the transient state.

Finally the dependence of the molar fraction on t_{res} and V_R was observed and compared with that simulated. Fig. 6 shows the pherograms observed for the MCA and PIC system upon varying the molar fraction of PIC from *ca.* 0.1 to 0.5 (the total amount was *ca.* 40 nmol and the pH of the solution was *ca.* 2.5). A small amount of SPADNS was added to the mixture. Apparently the mixed zones diminished at the same channels 31 and 32, suggesting that the resolution time was independent of the variation of the molar fraction of PIC. The boundary velocity of M/MP increased and that of MP/P decreased with increasing molar fraction of PIC. Consequently the mixed zones diminished at the same resolution time.

TABLE VIII

SIMULATED CONCENTRATION RATIO OF SAMPLES, R_E, pH OF ZONES AND EFFECTIVE MOBILITIES IN THE MIXED ZONE OF THE MONOCHLOROACETATE–PICRATE SYSTEM (1:1) AT pH_S = 2.5, 3.0 AND 3.6

For the operational system, see Table VII. Sample amounts: monochloroacetic acid (M), 20 nmol; picric acid (P), 18.68 nmol. $C^t_{P,MP}/C^t_{M,MP}$ = Ratio of the total concentrations of M and P in the mixed zone; $R_{E,MP}$ = ratio of potential gradient to that of the leading zone; pH_{MP} = pH of the mixed zone; $\bar{m}$ = effective mobility ($cm^2\ V^{-1}\ s^{-1}$).

	pH_S	*Simulated value**		
		Non-SPR	*SPR-II*	*SPR-III*
$C^t_{P,MP}/C^t_{M,MP}$	2.5	0.993	2.776	1.086
	3.0	–	1.490	1.062
	3.6	–	1.043	0.968
$R_{E,MP}$	2.5	2.360	2.460	2.369
	3.0	–	2.402	2.367
	3.6	–	2.365	2.357
pH_{MP}	2.5	3.830	3.835	3.830
	3.0	–	3.832	3.830
	3.6	–	3.830	3.830
$\bar{m}_{P,MP}$	2.5	29.44	29.46	29.44
	3.0	–	29.45	29.44
	3.6	–	29.44	29.44
$\bar{m}_{M,MP}$	2.5	35.35	35.39	35.35
	3.0	–	35.37	35.35
	3.6	–	35.35	35.34

* For definitions of the transient state models, see text.

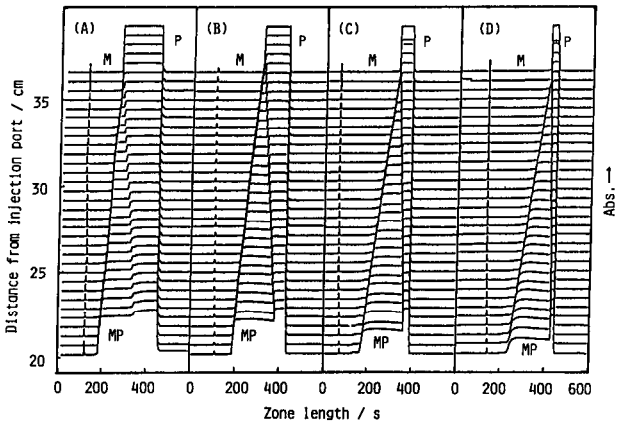

Fig. 6. Transient isotachopherogram of monochloroacetic acid (MCA) and picric acid (PIC) obtained by the use of the 32-channel UV-photometric detector. (A) 20.0 nmol MCA, 18.7 nmol PIC, (B) 26.7 nmol MCA, 12.4 nmol PIC; (C) 33.3 nmol MCA, 6.2 nmol PIC and (D) 36.4 nmol MCA, 3.4 nmol PIC. For the analytical conditions, see Fig. 4.

TABLE IX

OBSERVED AND SIMULATED RELATIVE VELOCITY AND RESOLUTION TIME FOR THE MONOCHLOROACETATE–PICRATE SYSTEM

For the operational system, see Table VII. I.D. of the separation tube = 0.54 mm. Sample amounts: monochloroacetic acid (M): picric acid (P) = 20.0:18.68 (1:1), 26.68:12.44 (2:1), 33.32:6.24 (5:1) and 36.36 nmol:3.40 nmol (10:1).

Molar fraction		*Simulated**				*Obs.***
		Non-SPR	*SPR-II**		*SPR-III**	*2.5*
			pH_S = *2.5*	*4.0*	*2.5*	
1:1	$V_{R,M/MP}$	0.913	0.953	0.911	0.917	0.923
	$V_{R,MP/P}$	1.096	1.145	1.094	1.101	1.097
	t_{res}(s)	1015	1892	1003	1072	1155
2:1	$V_{R,M/MP}$	0.886	0.927	0.885	0.891	0.896
	$V_{R,MP/P}$	1.063	1.113	1.061	1.069	1.055
	t_{res}(s)	1040	1624	1027	1084	1144
5:1	$V_{R,M/MP}$	0.860	0.891	0.859	0.864	0.875
	$V_{R,MP/P}$	1.031	1.069	1.030	1.036	1.036
	t_{res}(s)	1057	1353	1050	1086	1121
10:1	$V_{R,M/MP}$	0.848	0.868	0.848	0.850	0.847
	$V_{R,MP/P}$	1.017	1.041	1.016	1.020	1.009
	t_{res}(s)	1065	1047	1061	1082	1101

* For definitions of the transient state models, see text.

** The probable error in V_R was 0.001–0.004.

TABLE X

SIMULATED R_E VALUES, EFFECTIVE MOBILITIES AND CONCENTRATIONS OF ZONE CONSTITUENTS IN THE STEADY STATE ZONE AND THE TRANSIENT MIXED ZONE OF THE MONOCHLOROACETATE–PICRATE SYSTEM AT pH_L = 3.6 (25°C)

For operational system, see Table VII. For sample amount, see Table IX. pH_S^* = pH of sample zone actually interfacing with the mixed zone. For definition of other symbols, see Table VI.

	pH_S^*	R_E	pH	$\bar{m}_{MCA}$	$\bar{m}_{PIC}$	C^t_{MCA}	C^t_{PIC}	$\bar{m}_Q$	C^t_Q	I
Steady state zone										
MCA		2.16	3.821	35.1	–	3.66	–	12.6	8.68	3.32
PIC		2.59	3.841	–	29.3	–	3.09	12.2	8.33	3.08
Transient mixed zone										
1:1	3.47	2.35	3.829	35.3	29.4	1.78	1.59	12.4	8.51	3.21
2:1	3.40	2.28	3.826	35.3	29.4	2.40	1.07	12.5	8.57	3.25
5:1	3.33	2.22	3.823	35.3	29.4	3.03	0.54	12.6	8.63	3.28
10:1	3.30	2.19	3.822	35.3	29.4	3.32	0.30	12.6	8.66	3.30

Table IX shows the dependence of the molar fraction on the observed and the simulated boundary velocities and t_{res}. The observed values were the averages from three experiments at 25°C. The agreement between the observed and the values simulated by the SPR-III model was again very good.

Table X summarizes the simulated R_E values, effective mobilities and concentrations of the zone constituents of the MCA and PIC system at both the steady state and the transient state. A significant difference between the models used was found only for the estimates of the sample concentrations and potential gradient of the mixed zone MP, E_{MP}.

Thus, the overestimation by the transient state models SPR-I and SPR-II at low pH_S may be explained properly only by the pH perturbation at the initial stage. From the present work, an important conclusion was deduced that the properties of the mixed zone are regulated not only by those of the sample solution injected itself but also by those of the leading zone. As discussed, the simulated pH shift was large and it reduced considerably the pH_S effect in the separation process. The shift of the pH boundary in the sample solution injected might be observed by the use of an appropriate pH indicator; it was not observed in the present work because of the structural restriction of the apparatus.

Although the observed small pH dependence on t_{res}, etc., cannot be simulated by the non-SPR model, it seems that the approximation by thus model is not far from reality. Especially from the practical viewpoint, the applicability of the non-SPR model to the transient state may be highly rated, because the discrepancy between the observed and the simulated t_{res} was always small, not only for a pair of a strong acid and a weak acid but also for a pair of weak acids.

We have investigated a convenient model to estimate the resolution time of samples on the basis of the zone lengths, concentrations, etc., at the steady state, which can be simulated exactly. The usefulness of the non-SPR model will be reported in a subsequent paper dealing with two- and three-component systems.

ACKNOWLEDGEMENTS

T.H. thanks the Ministry of Education, Science, and Culture of Japan for support of the part of this work under a Grant-in-Aid for Scientific Research (No. 61540423). We are also grateful for the helpful suggestions made by Dr. F. M. Everaerts (Eindhoven University of Technology, The Netherlands).

REFERENCES

1 T. Hirokawa, K. Nakahara and Y. Kiso, *J. Chromatogr.*, 463 (1989) 39–49.
2 G. Brouwer and G. A. Postema, *J. Electrochem. Soc.*, 117 (1970) 874.
3 J. Vacik and V. Fidler, in F. M. Everaerts (Editor), *Analytical Isotachophoresis*, Elsevier, Amsterdam, 1981, pp. 19–24.
4 F. E. P. Mikkers, F. M. Everaerts and J. A. F. Peek, *J. Chromatogr.*, 168 (1979) 293.
5 F. E. P. Mikkers, F. M. Everaerts and J. A. F. Peek, *J. Chromatogr.*, 168 (1979) 317.
6 R. A. Alberty, *J. Am. Chem. Soc.*, 72 (1950) 2361.
7 T. Hirokawa and Y. Kiso, *Shimadzu Kagaku Kikai News*, 25 (1984) 24.
8 T. Hirokawa and Y. Kiso, *J. Chromatogr.*, 242 (1983) 227.
9 R. A. Robinson and R. H. Stokes, *Electrolyte solutions*, Butterworths, London, 1959.
10 T. M. Jovin, *Biochemistry*, 12 (1973) 871.
11 T. M. Jovin, *Biochemistry*, 12 (1973) 879.
12 T. M. Jovin, *Biochemistry*, 12 (1973) 890.
13 H. Svenson, *Acta Chem. Scand.*, 2 (1948) 841.